Compositional Design of Spontaneous Heterointerface Modulators for Perovskite Solar Cells Allowing a Broad Process Window

Naoyuki Nishimura, Hiroyuki Kanda, Takurou N. Murakami*

National Institute of Advanced Industrial Science and Technology (AIST), 1-1-1 Higashi, Tsukuba, Ibaraki 305-8565, Japan

***Corresponding Author**

Naoyuki Nishimura. E-mail: naoyuki-nishimura@aist.go.jp

ABSTRACT

Spontaneous heterointerface modulation techniques have significantly contributed to the rapid development of perovskite solar cells (PSCs), and alkyl-primary-ammonium bis(trifluoromethanesulfonyl)imides (RA–TFSIs), whose archetype is *n*-octylammonium bis(trifluoromethanesulfonyl)imides (OA–TFSI), have recently emerged as functional additives for hole transport materials (HTMs). RA–TFSIs are designed to allow spontaneous perovskite passivation via the HTM deposition process; leveraging the high reactivity of RA cations toward the perovskite surface, these additives spontaneously and effectively suppress the defects over the perovskite surface and thereby enhance photovoltaic (PV) performance. Moreover, this perovskite passivation negates the need for conventional post-passivation processes, thereby improving the fabrication efficiency of PSCs. Although the advantages of these PSC fabrication processes have been less discussed than methods aimed at enhancing PV performance, they are crucial for further advancement of PSCs, especially in the context of spontaneous heterointerface modulation techniques. A key aspect is the concentration sensitivity of RA–TFSI; excessive OA–TFSI in the HTM solution leads to some OA cations failing to attach to the perovskite surface during spontaneous passivation, remaining in the HTM core and hindering carrier collection. To address this issue, we herein developed RA–TFSIs and synthesized ethylammonium bis(trifluoromethanesulfonyl)imide (EA–TFSI) for the first time. EA–TFSI not only enhanced the PV properties of PSCs but also significantly mitigated the concentration sensitivity owing to its small cation size, reducing the risk of poor carrier collection. In the case of OA–TFSI, increasing its concentration to twice the optimal amount decreased power conversion efficiency (PCE) by 14%, accompanied by drops in fill factor (FF). However, upon EA–TFSI addition, PCE decreased by only 4%, with FF values remaining unchanged (i.e., nearly 100% retention). This research

offers insights into designing nascent yet potent spontaneous heterointerface modulators for PSCs, including RA–TFSI, to facilitate a broad process window, which is critical yet rarely discussed aspect. Therefore, this study will contribute to the further development of PSCs.

INTRODUCTION

Perovskite solar cells (PSCs) have attracted considerable research attention over the past decade,[1, 2] and a recent and potent advancement is spontaneous heterointerface modulation in PSCs.[3-9] PSCs comprise multiple layers (e.g., an n–i–p cell structure consists of a transparent conductor, an electron transport material, a perovskite photoabsorber, a hole transport material (HTM), and a metal conductor); Spontaneous heterointerface modulators (SHMs)[3-7] effectively improve the heterointerface properties during the deposition process, likely exploiting the driving energy of a highly exothermic reaction between SHM components and a component layer in PSCs (e.g., strong chemical interaction between them). Thus, development of novel SHM material design can promote further advancement of PSCs.

A significant development in SHM technology is the emergence of alkyl-primary-ammonium bis(trifluoromethanesulfonyl)imide (RA–TFSI) additives for HTMs.[3-6] The prime advantages of this technique are (i) the absence of Li species, which is detrimental to the PV performance of PSCs[10-14], in contrast to the most commonly used Li–TFSI additive, and (ii) spontaneous perovskite passivation during the HTM deposition process. In particular, spontaneous passivation via HTM deposition is not attainable by other Li-free HTM additives[13-24] and represents a unique property of RA–TFSIs. In the case of *n*-octylammonium TFSI (OA–TFSI), an archetypal material, owing to the high adsorption energy of OA cations on the perovskite surface (e.g., 1.88 eV[25]), OA cations spontaneously passivate the perovskite surface during the deposition of an HTM solution containing the OA–TFSI additive.[3, 4, 6] As a result, the formation of defects on the perovskite surface is effectively suppressed by spontaneous passivation; thus, using the OA–TFSI additive considerably enhances the PV properties of PSCs. Although the conventional passivation of the perovskite layer with passivator salts requires a post-passivation process[25-39], adding RA–TFSIs to the HTM solution helps avoid the additional passivation step, increasing PSC fabrication efficiency. To realize the potential of this spontaneous perovskite passivation technique using RA–TFSIs, strategies that focus on advancing manufacturing processes, such as those aimed at achieving a broad process window in addition to high process efficiency, are ideally implemented. However, unlike the techniques for PV performance enhancement, such strategies have not been explored in detail.

One of the parameters that can be improved using this approach is the concentration sensitivity of RA–TFSIs in the HTM solution. When excess OA–TFSI is added to the HTM solution, for instance, the PV performance degrades in relation to that at the optimal OA–TFSI amount.[3, 4, 6] This occurs presumably because some OA cations cannot attach to the perovskite surface during the spontaneous passivation process and thereby remain in the HTM core.[3] Consequently, the presence of OA cations in the HTM most likely inhibits hole transfer via the HTM. This phenomenon is most likely a common trend not only for RA–TFSIs but also for other SHMs because the excessive addition of a component that exhibits spontaneous heterointerface modulation in SHMs (e.g., OA in the case of OA-TFSI) can lead to the formation of unreacted (or uncoordinated) components, which prevents the construction of efficient PSCs due to the limited number of substances that can react with the SHM (e.g., sites capable to adsorption of OA over the perovskite surface). As this problem has seldom been discussed, its possible solutions can provide crucial guidelines for developing SHMs for PSCs.

Herein, we propose the design of an RA–TFSI composite to solve the concentration sensitivity problem; a newly synthesized ethylammonium TFSI (EA–TFSI) as an additive for HTM solutions that exhibit effective spontaneous perovskite passivation via HTM deposition with a significantly broader process window than those of conventional RA–TFSIs such as OA–TFSI. While the effective perovskite passivation properties increase the PCE up to 22.6%, the smaller size of the EA cation in EA–TFSI than those of conventional cations (e.g., OA) effectively decreases the concentration sensitivity and expands the process window (Figure 1). This study provides novel insights into the spontaneous perovskite passivation process and paves the way for developing highly efficient SHMs for PSCs, including RA–TFSI spontaneous passivators.

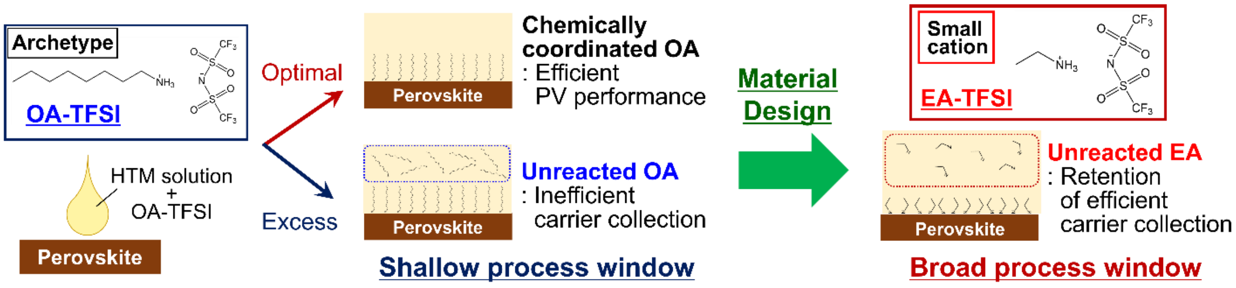

Figure 1. Scheme of the compositional design of spontaneous heterointerface modulators allowing a broad process window (cases of OA-TFSI[3, 4, 6] and EA-TFSI)

RESULTS AND DISCUSSION

Figure 2a shows the cross-sectional image of the PSC with the EA–TFSI additive, confirming the standard configuration of the fluorine-doped tin oxide (FTO)/TiO_2/perovskite/Spiro-OMeTAD/Au n–i–p structure. A similar structure was observed in the PSC with Li–TFSI (Figure S1); however, the use of different additives resulted in different material characteristics, including PV performance. The surface analysis of the perovskite layer via X-ray photoelectron spectroscopy

(XPS) strongly suggests the presence of EA cations on the surface of the perovskite using the EA–TFSI additive as well as the occurrence of spontaneous perovskite passivation. Figure 2b shows the XPS profiles of the pristine perovskite (reference) and perovskite with EA–TFSI (target). Two peaks at 288.3 and 285 eV in both spectra, corresponding to the C=N and C–C + C–H species,[3, 29] respectively, are observed. The sample with EA–TFSI exhibits a larger peak at 284.5 eV corresponding to the C–C and C–H species, which likely results from EA cations. The small peak at 285 eV obtained for the pristine perovskite originates from carbon contaminants, which are generally detected by XPS. As the presence of an aliphatic moiety (i.e., EA in this study) rendered the perovskite surface hydrophobic,[26] contact angle (CA) measurement with water droplets on the perovskite surface was conducted. Figure 2c shows the CA measurement results for the perovskite layer after HTM removal using Li–TFSI (reference) and EA–TFSI (target). The sample with EA–TFSI exhibits a higher CA (57 ± 2°) than that with Li–TFSI (43 ± 3°). This indicates that using the EA–TFSI additive for the HTM rendered the perovskite surface hydrophobic and confirmed the spontaneous perovskite passivation via HTM deposition.

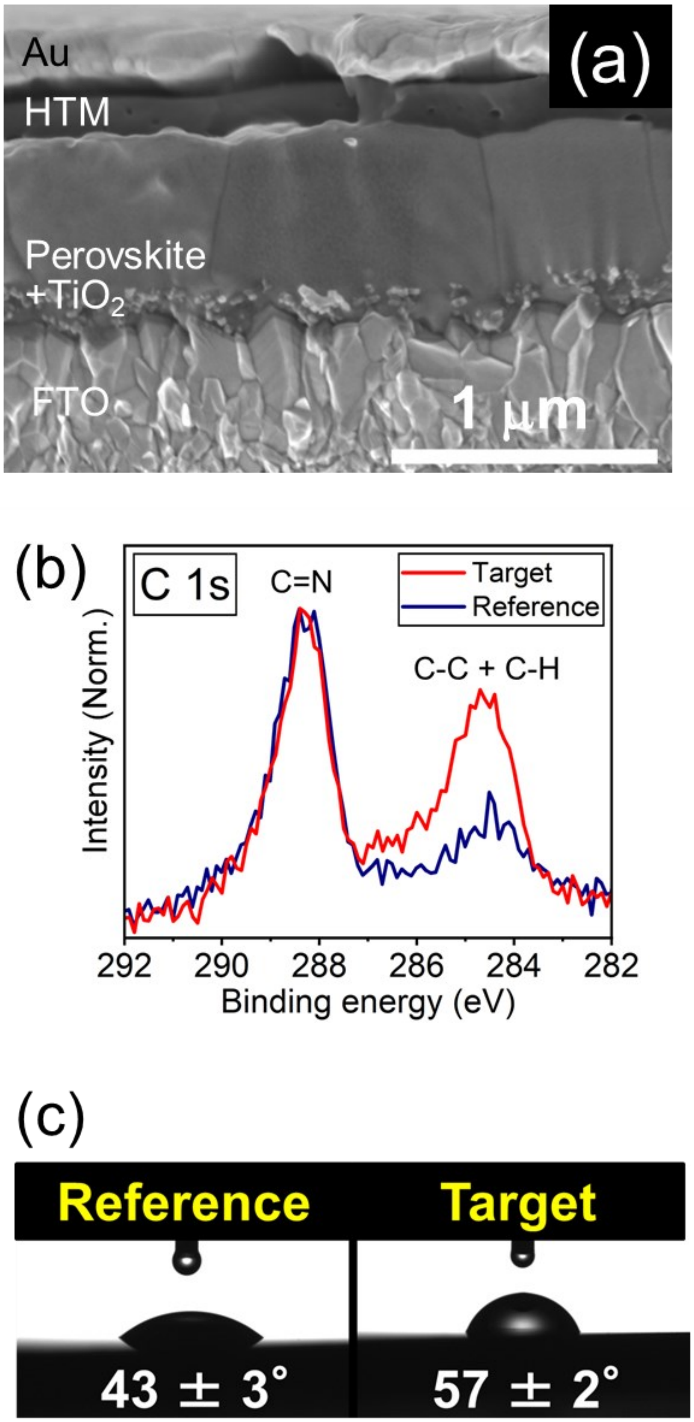

Figure 2. (a) Cross-sectional SEM image of the PSC with EA–TFSI. (b) XPS profiles and (c) CA measurement results obtained for the reference and target samples.

As perovskite passivation affects carrier dynamics, the photoluminescence (PL) lifetimes were measured. Figures 3a and b depict the PL lifetimes of the HTM/perovskite bilayer samples with Li–TFSI and EA–TFSI and perovskite monolayer measured after the removal of the HTM layer, respectively. The bilayer sample with EA–TFSI exhibits a shorter lifetime (5.2 ± 0.1 ns) than the sample with Li–TFSI (7.5 ± 0.1 ns), suggesting that perovskite passivation with EA cations facilitates carrier injection from the perovskite to HTM. This effect is presumably due to the cationic passivation with EA, leading to a p-type character of the resulting perovskite surface. [3, 31] The perovskite monolayer sample with EA–TFSI demonstrates a longer PL lifetime (67.3 ± 0.2 μs) than that of the monolayer sample with Li–TFSI (52.6 ± 0.1 μs), indicating that EA cations spontaneously passivated the perovskite layer during the HTM deposition process and suppressed the formation of defects over the perovskite surface,[3, 8] similar to RA–TFSI spontaneous passivators. [4-6]

Another advantage of the spontaneous perovskite passivation via HTM deposition is the absence of the counter cations in the HTM core, facilitating the formation and stabilization of HTM cationic radicals via the reaction with TFSI anions.[3, 6] In Spiro-OMeTAD, the singly occupied molecular orbital corresponding to the cationic radicals is located below the highest occupied molecular orbital;[10] therefore, the high ionization energy (IE) of the HTM layer suggests a higher concentration of cationic radicals. To investigate the effect of the enhanced Spiro-OMeTAD cationic radical formation using EA–TFSI, the IE of the HTM layer was determined (Table 1). Even at a low EA–TFSI concentration (5.52 eV, 18 mM (optimal)), the IE is slightly higher than that of the sample with Li–TFSI (5.50 eV, 48 mM), indicating that the spontaneous perovskite passivation promotes the formation and stabilization of Spiro-OMeTAD cationic radicals, which is consistent with the effects of other RA–TFSI spontaneous perovskite passivators. [3, 4, 6]

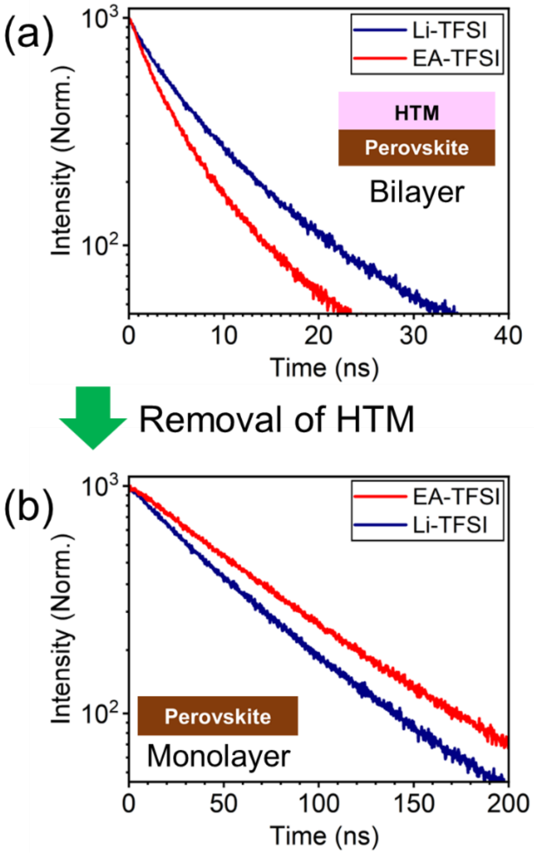

Figure 3. PL lifetimes of the samples with Li–TFSI and EA–TFSI: (a) HTM/perovskite bilayer and (b) perovskite monolayer.

Table 1. IEs of the HTMs

Additive	TFSI concentration (mM)	IE (eV)
EA–TFSI	18	5.52
Li–TFSI	48	5.50

Figure 4 shows the PV performance of the PSCs with Li–TFSI and optimal EA–TFSI. The PSCs with EA–TFSI exhibit superior PV characteristics to those with Li–TFSI, owing to the spontaneous passivation effects. The PV parameter distributions (Figure 4a) and average values (Table 2) indicate that the PSCs with EA–TFSI possess substantially higher PCEs (21.7 ± 1.0% in the backward scan) than those with Li–TFSI (19.1 ± 1.8 in the backward scan). Similarly, for the highest-performance cells, the target PSC resulted in a considerably higher PCE (up to 22.6%) than the reference PSC (up to 21.3%; Table 2). The PV performance evaluated in the forward scan showed similar trends (Figure S2 and Table 2). This increase in PCE of the PSCs with EA–TFSI is primarily attributed to the increase in open-circuit voltage (V_{oc}) from 1.06 to 1.11 V for the highest-performance cells in the backward scan, confirming the effectiveness of the spontaneous perovskite passivation. It is noteworthy here that the EA-based effective perovskite passivation is consistent with conventional passivation using EA iodide[26, 27] via an additional post-treatment step. It is also noted that short-circuit current (J_{sc}) in the J–V curve of the highest-performance cell with EA–TFSI (26.1 mA cm^{-2} (Table 2)) matches the integrated J_{sc} value estimated from the corresponding external quantum efficiency (EQE) curve (25.2 mA cm^{-2}, difference: within 4%) (Figure 4b). Figure 4c shows the quasi-steady-state PCE (QSS–PCE) of the highest-performance cell with EA–TFSI. Its estimated value is 22.3%, which is nearly equal to the PCE obtained in the backward scan (22.6%); hence, the parameters evaluated in the backward scan represent the actual PV performance, which is in good agreement with the case of other RA–TFSI additives combined with Spiro-OMeTAD HTM and another HTM (polytriarylamine: PTAA), indicating a common trend observed for the RA-TFSI spontaneous perovskite passivators.[3-6] Consequently, although the size of EA cations is much smaller than that of conventional RA cations in RA–TFSIs, the EA–TFSI additive effectively improves the PV performance in relation to the Li–TFSI additive owing to the spontaneous perovskite passivation effects.

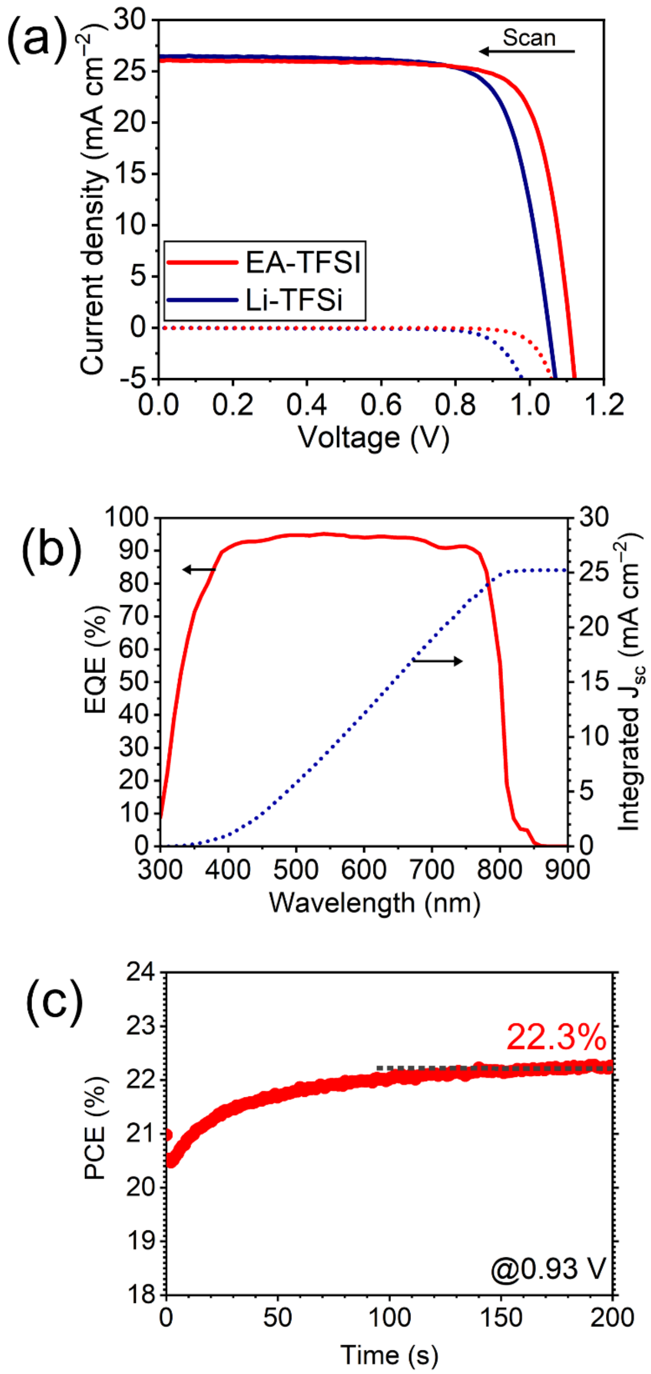

Figure 4. (a) J–V curves of the highest-performance PSCs with EA–TFSI and Li–TFSI recorded in the backward scan (forward scan: Figure S2). (b) EQE spectrum of the highest-performance PSC with EA–TFSI. (c) QSS–PCE curve of the highest-performance PSC with EA–TFSI obtained at 0.93 V

Table 2. PV parameters of the PSCs with optimal EA–TFSI and Li–TFSI

HTM additive	Scan	Average / Best	J_{sc} (mA/cm^2)	V_{oc} (V)	FF	PCE (%)
EA–TFSI	Backward	Best	26.1	1.11	0.78	22.6
		Average	25.7 ± 0.3	1.10 ± 0.01	0.77 ± 0.04	21.7 ± 1.0
	Forward	Best	26.1	1.08	0.71	20.1
		Average	25.7 ± 0.3	1.06 ± 0.03	0.69 ± 0.04	18.8 ± 1.3
Li–TFSI	Backward	Best	26.5	1.06	0.76	21.3
		Average	26.3 ± 0.4	1.03 ± 0.02	0.71 ± 0.05	19.1 ± 1.8
	Forward	Best	26.5	1.00	0.65	17.1
		Average	26.3 ± 0.4	0.95 ± 0.04	0.59 ± 0.06	14.7 ± 2.0

The spontaneous perovskite passivation effects of the EA–TFSI additive are similar to those of other RA–TFSIs; however, EA–TFSI demonstrates a lower concentration sensitivity. Figure 5a and Table 3 show the dependences of various PV parameters on the EA–TFSI concentration. Figures 5b and c depict the RA–TFSI (EA–TFSI in the present work and OA–TFSI in a literature study[6]) concentration dependences on the relative average PCE and relative average FF, respectively. With an increase in the EA–TFSI concentration from 6 to 18 mM, the PCE increases from 16.7 ± 0.7% to 21.7 ± 1.0% and reaches the optimal value. After further increasing the EA–TFSI concentration to 48 mM, which is 2.7 times higher than the optimal concentration, the PCE slightly decreases to 20.9 ± 0.5% (by relative 4% decrease); however, it does not exhibit a significant drop, unlike that of OA–TFSI. As shown in Figure 5b, with an increase in the OA-TFSI concentration from optimal 24 mM to excess 48 mM, the PCE decreased by relative 14%,[6] which is substantially larger than that with EA-TFSI.

In more details, the PCE slightly decreases from 21.7 ± 1.0% to 20.9 ± 0.5% with an increase in the EA–TFSI concentration from 18 to 48 mM, which is attributed to the slightly decreased V_{oc} value from 1.10 ± 0.01 to 1.05 ± 0.01 V (Table 3, relative 5% decrease: Figure S3). As EA–TFSI is in the solid state at room temperature, the co-addition of TBP is required for its dissolution. Meanwhile, a higher concentration of TBP can prevent spontaneous perovskite passivation by EA cations as TBP can directly cause chemical attachment to perovskite surface[40-44] and thereby decreases the V_{oc} value.[6] Therefore, the slight decrease in V_{oc} with increasing EA–TFSI concentrations accompanied by an increase in the TBP concentration is presumably due to the prevention of spontaneous perovskite passivation at high TBP concentrations. This trend (i.e., decreased V_{oc} with increasing RA-TFSI concentration accompanying an increase in TBP concentration) is also observed for other RA–TFSI spontaneous perovskite passivators.[3, 5, 6] For example, with an increase in the OA–TFSI concentration from 24 to 48 mM, V_{oc} decreases from 1.12 ± 0.01 to 1.06 ± 0.02 V (Figure S3: relative 5% decrease).[6]

However, the FF values of the PSCs with EA–TFSI remained almost the same at 0.77 between the EA–TFSI concentrations of 18 and 48 mM, corresponding to a nearly 100% retention (Figure 5c). In stark contrast, the PSCs with OA–TFSI exhibited a significant decrease in FF by 7% with an increase in the OA–TFSI concentration from 24 to 48 mM (Figure 5c).[6] The same trend (an FF drop with increasing RA–TFSI concentration) was also observed in previous studies using other RA-TFSIs spontaneous perovskite passivators.[3-6] This difference between the FF trends is attributed to the difference in the cation structure because the addition of Li–TFSI within the concentration range employed in this work (up to 48 mM) did not result in such a significant detrioration;[3, 10, 45] hence, increasing the TFSI anion concentration does not decrease the FF value. The observed FF drop at high OA–TFSI concentrations can be attributed to the remaining OA cations in the HTM core. When an excessive amount of OA–TFSI is added to the HTM solution, some OA cations cannot attach to the perovskite surface during the spontaneous passivation process, and the presence of OA cations in the HTM most likely hinders the hole transfer via the HTM, leading to an FF drop.[3] Therefore, based on this assumption, the FF magnitude decreases with an increase in the RA–TFSI concentration and depends on the RA–TFSI cation structure; a small cation size will be advantageous for mitigating the FF decrease with increasing RA–TFSI concentration. The use of EA–TFSI in the present work confirmed this assumption; owing to the small EA cation size, the remaining EA cations in the HTM core affected hole collection only negligibly with the addition of excess EA–TFSI (in contrast to OA–TFSI addition), thereby demonstrating the low FF sensitivity to the EA–TFSI concentration. Therefore, the proposed mechanism of the RA–TFSI concentration sensitivity is supported by the results of this work; the remaining RA cations in the HTM core with excess RA–TFSI may potentially prevent hole collection; however, the use of smaller RA cations (e.g., EA in this work) can address this issue.

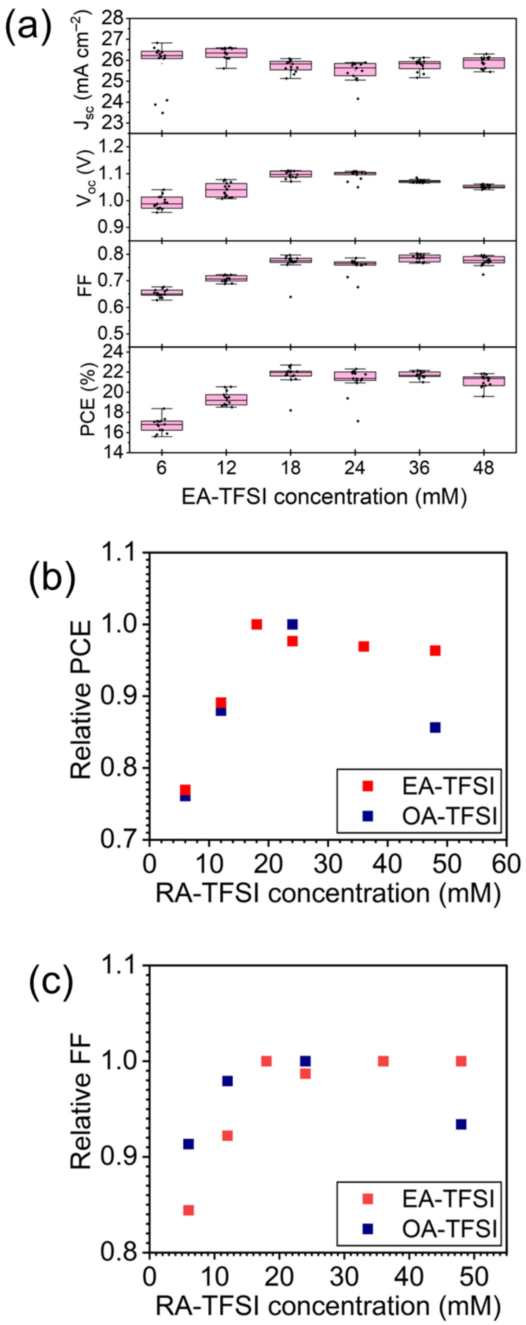

Figure 5. RA–TFSI concentration dependence on the PV properties of PSCs. (a) Variations of the absolute values with the EA–TFSI concentration. Relative (b) PCE and (c) FF values of EA–TFSI and OA–TFSI.

Table 3. EA-TFSI concentration dependence on the PV parameters

EA-TFSI concentration (mM)	J_{sc} (mA/cm^2)	V_{oc} (V)	FF	PCE (%)
6	25.8 ± 1.0	0.99 ± 0.02	0.65 ± 0.01	16.7 ± 0.7
12	26.3 ± 0.3	1.04 ± 0.02	0.71 ± 0.01	19.3 ± 0.7
18	25.7 ± 0.3	1.10 ± 0.01	0.77 ± 0.04	21.7 ± 1.0
24	25.5 ± 0.5	1.10 ± 0.02	0.76 ± 0.03	21.2 ± 1.3
36	25.5 ± 0.4	1.06 ± 0.01	0.77 ± 0.01	21.0 ± 0.6
48	25.8 ± 0.5	1.05 ± 0.01	0.77 ± 0.01	20.9 ± 0.5

CONCLUSION

A method for spontaneous perovskite passivation via HTM deposition with a broad process window was proposed in this study using a newly synthesized EA–TFSI additive for the HTM solution. The EA–TFSI additive enabled spontaneous perovskite passivation during HTM deposition similar to conventional RA–TFSI additives such as OA–TFSI, thereby effectively improving the PV performance and increasing PCE up to 22.6%. In other conventional RA–TFSI perovskite passivators such as OA–TFSI, the PSC properties are sensitive to their concentration owing to the large RA cation sizes: when excess OA–TFSI of twice the optimal amount was added to the HTM solution, the FF value decreases by relative 7% presumably owing to the large OA cations that remained in the HTM core and hampered hole collection, which decreased the PCE by 14%. However, EA–TFSI significantly mitigated the concentration sensitivity by reducing the risk of poor carrier collection when it remained in the HTM core because of its small cation size; therefore, at an EA–TFSI concentration two times higher than the optimal amount, only a 4% decrease in PCE was observed, while the FF value remained unchanged (i.e., almost 100%

retention). The observed concentration insensitivity led to a broad process window, which will mitigate the difficulty of manufacturing PSCs in addition to exploiting the enhanced process efficiency using the RA–TFSI spontaneous perovskite passivator (i.e., avoiding the conventional passivation process).

In addition to RA–TFSIs, the obtained insights regarding the material design also contributes to the development of other series of SHMs as the concentration sensitivity addressed in this work is a common issue for SHMs in principle, although this feature has seldom been discussed. Therefore, the present research has the potential to pave the way for development of highly efficient SHMs, including RA–TFSI spontaneous perovskite passivators, characterized by broad process windows. This contribution, in turn, fosters the ongoing progress of PSCs.

Experimental Section

Materials

All materials were of reagent grade and used as received. Lead iodide (PbI_2), ethylamine, and HTFSI were purchased from Tokyo Chemical Industry Co., Ltd. Formamidine hydroiodide (FAI) and mesoporous titanium oxide (m-TiO_2; 30NR-R) were obtained from Great Cell Solar Technology. Methylammonium chloride (MACl) was procured from Xian Polymer Co., Ltd. All other reagents were obtained from Sigma–Aldrich. FTO-coated transparent glass (thickness: 1.6 mm, sheet resistance: $\leq 10\ \Omega\ cm^{-2}$) was purchased from Nippon Sheet Glass.

Synthesis of EA–TFSI

EA–TFSI was synthesized via a neutralization method. First, ethanol solutions with the same volume and molar concentration of ethylamine and HTFSI were prepared. Subsequently, the phenylethylamine solution was added dropwise to the HTFSI solution while stirring in an ice bath. After stirring for 2 h, ethanol was removed for 3 h using a vacuum evaporator. The resulting solid material was EA–TFSI, as confirmed via NMR spectroscopy (Figure S4 and S5). EA–TFSI was in the solid state at room temperature; however, its melting point (318 K: Figure S6) was close to room temperature and within the range corresponding to that of an ionic liquid definition (<373 K)[46].

Synthesis of $FAPbI_3$ powder

$FAPbI_3$ powder was synthesized as a thin film precursor using a previously reported method.[3, 38, 47] Briefly, 0.8 M of FAI and PbI_2 powders were dissolved in 2-methoxyethanol, and the resulting solution was subsequently heated to 393 K for 1 h under stirring. The precipitated black particles were immediately collected via filtration and heated to 423 K for 30 min. The resulting black powder was dried by evacuation at room temperature for 1 h.

Solar cell fabrication

The PSCs were prepared using conventional methods, with some modifications.[1] A TiO_2 compact layer (~50 nm) was coated onto an FTO glass substrate via the spray pyrolysis of a 4 vol.% titanium diisopropoxide bis(acetylacetate)/ethanol solution and then placed on a hotplate at 523 K.

Subsequently, an m-TiO_2 layer was deposited by spin coating a TiO_2 paste diluted with ethanol onto the substrate surface at 5000 rpm for 10 s, followed by heating the substrate to 773 K for 30 min.

The $FAPbI_3$ perovskite layer was deposited onto as-prepared TiO_2/FTO via spin coating in a dry room (temperature: 291 K, dew point: <243 K). A 1.8 M $FAPbI_3$ precursor solution was prepared by dissolving the synthesized $FAPbI_3$ powder and 40 mol.% (for $FAPbI_3$) of MACl in a mixed solution of *N,N*-dimethylformamide and dimethyl sulfoxide (4:1 v/v). The TiO_2/FTO substrate was spin-coated with the precursor solution at 6000 rpm for 50 s. During spin coating, 1 mL of chlorobenzene was added dropwise after spinning for 10 s.

The HTM layer was deposited by spin coating a solution containing Spiro-OMeTAD and additives at 3000 rpm for 30 s in a dry room. The HTM solution with the EA–TFSI additive was prepared by dissolving 70 mM Spiro-OMeTAD in chlorobenzene and mixing desired amounts of EA–TFSI and 4 times more of TBP. For the HTM solution with the Li–TFSI additive, 70 mM Spiro-OMeTAD, 48 mM Li–TFSI, and 210 mM TBP were dissolved in chlorobenzene. Finally, an Au conductor layer (~200 nm) was deposited via thermal evaporation. Accordingly, a PSC with the n-i-p standard configuration was obtained (Figure 2a).

Current–voltage curve analysis

The current–voltage curves were recorded using a source meter (R6243, ADVANTEST) and class A solar simulator (XIL-05B100KP, Seric Co.) with a mismatch factor of <25%, calibrated using a Si-reference cell equipped with a KG-5 filter to generate the AM1.5G spectrum (100 mW cm^{-2})

at room temperature (~298 K) in an ambient atmosphere. The current–voltage scan was performed at a constant speed of 100 mV s^{-1} under simulated sunlight radiation using a sample mask with an aperture area of 0.119 cm^2. Before each measurement, an antireflection sheet was pasted onto the glass side of the cell. No pre-bias was applied prior to the measurements. More than 15 samples were examined under various target and reference conditions, and the best samples were selected. The average values of the measured solar cell parameters with standard deviation were calculated.

Characterization of EA–TFSI

NMR spectroscopy was performed using a JNM-ECZ400S/L1 spectrometer (JEOL Co., Ltd.). Thermal stability was measured using a thermogravimetry-differential thermal analysis (TG-DTA) instrument (STA200RV, Hitachi High-Tech Science Co.) at a 10 K/min scan rate under nitrogen flow.

Acknowledgements

This article is based on results from a project, JPNP21016, commissioned by the New Energy and Industrial Technology Development Organization (NEDO).

Author contributions

Naoyuki Nishimura: Conceptualization, Project administration, Investigation, Resources, Formal analysis, Writing – original draft, Writing – review & editing, **Hiroyuki Kanda:** Writing – review & editing, **Takurou N. Murakami:** Supervision, Funding acquisition, Writing – review & editing

Notes

There are no conflicts to declare.

References

(1) Lee, M. M.; Teuscher, J.; Miyasaka, T.; Murakami, T. N.; Snaith, H. J. Efficient Hybrid Solar Cells Based on Meso-Superstructured Organometal Halide Perovskites. *Science* **2012**, *338*, 643-647.

(2) Kim, H. S.; Lee, C. R.; Im, J. H.; Lee, K. B.; Moehl, T.; Marchioro, A.; Moon, S. J.; Humphry-Baker, R.; Yum, J. H.; Moser, J. E.; et al. Lead Iodide Perovskite Sensitized All-Solid-State Submicron Thin Film Mesoscopic Solar Cell with Efficiency Exceeding 9%. *Sci. Rep.* **2012**, *2*, 591.

(3) Nishimura, N.; Tachibana, H.; Katoh, R.; Kanda, H.; Murakami, T. N. Archetype-Cation-Based Room-Temperature Ionic Liquid: Aliphatic Primary Ammonium Bis(trifluoromethylsulfonyl)imide as a Highly Functional Additive for a Hole Transport Material in Perovskite Solar Cells. *ACS Appl. Mater. Interfaces* **2023**, *15*, 44859-44866.

(4) Kim, Y.; Kim, G.; Park, E. Y.; Moon, C. S.; Lee, S. J.; Yoo, J. J.; Nam, S.; Im, J.; Shin, S. S.; Jeon, N. J.; et al. Alkylammonium Bis(trifluoromethylsulfonyl)imide as a Dopant in the Hole-Transporting Layer for Efficient and Stable Perovskite Solar Cells. *Energy Environ. Sci.* **2023**, *16*, 2226-2238.

(5) Nishimura, N.; Kanda, H.; Katoh, R.; Murakami, T. N. Thermally Stable Phenylethylammonium-based Perovskite Passivation: Spontaneous Passivation with Phenylethylammonium Bis(trifluoromethylsulfonyl)imide under Deposition of PTAA for Enhancing Photovoltaic Performances of Perovskite Solar Cells. *J. Mater. Chem. A* **2024**, DOI: 10.1039/D4TA02036G

(6) Nishimura, N.; Tachibana, H.; Katoh, R.; Kanda, H.; Murakami, T. N. Reactivity Manipulation of Ionic Liquid Based on Alkyl Primary Ammonium: Protonation Control Using Pyridine Additive for Effective Spontaneous Passivation of Perovskite via Hole Transport Material Deposition *ChemRxiv* **2024**. DOI: 10.26434/chemrxiv-2024-ts5k7

(7) Wang, W.; Wei, K.; Yang, L.; Deng, J.; Zhang, J.; Tang, W. Dynamic Self-Assembly of Small Molecules Enables the Spontaneous Fabrication of Hole Conductors at Perovskite/Electrode

Interfaces for Over 22% Stable Inverted Perovskite Solar Cells. *Mater. Horiz.* **2023**, *10*, 2609-2617.

(8) Nishimura, N.; Behera, R. K.; Katoh, R.; Kanda, H.; Murakami, T. N.; Matsuzaki, H. Unveiled Effects of Methylammonium Chloride Additives on Formamidinium Lead Halide: Expediting Carrier Injection from the Photoabsorber to Carrier Transport Layers through Spontaneously Modulated Heterointerfaces in Perovskite Solar Cells. *J. Mater Chem. C* **2024**, DOI: 10.1039/D4TC00843J

(9) Bai, S.; Da, P.; Li, C.; Wang, Z.; Yuan, Z.; Fu, F.; Kawecki, M.; Liu, X.; Sakai, N.; Wang, J. T.; et al. Planar Perovskite Solar Cells with Long-Term Stability Using Ionic Liquid Additives. *Nature* **2019**, *571*, 245-250.

(10) Schloemer, T. H.; Christians, J. A.; Luther, J. M.; Sellinger, A. Doping Strategies for Small Molecule Organic Hole-Transport Materials: Impacts on Perovskite Solar Cell Performance and Stability. *Chem. Sci.* **2019**, *10*, 1904-1935.

(11) Li, Z.; Xiao, C.; Yang, Y.; Harvey, S. P.; Kim, D. H.; Christians, J. A.; Yang, M.; Schulz, P.; Nanayakkara, S. U.; Jiang, C.-S.; et al. Extrinsic Ion Migration in Perovskite Solar Cells. *Energy Environ. Sci.* **2017**, *10*, 1234-1242.

(12) Tan, B.; Raga, S. R.; Chesman, A. S. R.; Fürer, S. O.; Zheng, F.; McMeekin, D. P.; Jiang, L.; Mao, W.; Lin, X.; Wen, X.; et al. LiTFSI‐Free Spiro‐OMeTAD‐Based Perovskite Solar Cells with Power Conversion Efficiencies Exceeding 19%. *Adv. Ener. Mater.* **2019**, *9*, 1901519.

(13) Seo, J.-Y.; Kim, H.-S.; Akin, S.; Stojanovic, M.; Simon, E.; Fleischer, M.; Hagfeldt, A.; Zakeeruddin, S. M.; Grätzel, M. Novel p-Dopant Toward Highly Efficient and Stable Perovskite Solar Cells. *Energy Environ. Sci.* **2018**, *11*, 2985-2992.

(14) Seo, J. Y.; Akin, S.; Zalibera, M.; Preciado, M. A. R.; Kim, H. S.; Zakeeruddin, S. M.; Milić, J. V.; Grätzel, M. Dopant Engineering for Spiro‐OMeTAD Hole‐Transporting Materials towards Efficient Perovskite Solar Cells. *Adv. Funct. Mater.* **2021**, *31*, 2102124.

(15) Abate, A.; Hollman, D. J.; Teuscher, J.; Pathak, S.; Avolio, R.; D'Errico, G.; Vitiello, G.; Fantacci, S.; Snaith, H. J. Protic Ionic Liquids as p-Dopant for Organic Hole Transporting Materials and Their Application in High Efficiency Hybrid Solar Cells. *J. Am. Chem. Soc.* **2013**, *135*, 13538-13548.

(16) Zhang, H.; Shi, Y.; Yan, F.; Wang, L.; Wang, K.; Xing, Y.; Dong, Q.; Ma, T. A Dual Functional Additive for the HTM Layer in Perovskite Solar Cells. *Chem. Commun.* **2014**, *50*, 5020-5022.

(17) Caliò, L.; Salado, M.; Kazim, S.; Ahmad, S. A Generic Route of Hydrophobic Doping in Hole Transporting Material to Increase Longevity of Perovskite Solar Cells. *Joule* **2018**, *2*, 1800-1815.

(18) Zhang, J.; Zhang, T.; Jiang, L.; Bach, U.; Cheng, Y.-B. 4-tert-Butylpyridine Free Hole Transport Materials for Efficient Perovskite Solar Cells: A New Strategy to Enhance the Environmental and Thermal Stability. *ACS Ener. Lett.* **2018**, *3*, 1677-1682.

(19) Zhou, X.; Hu, M.; Liu, C.; Zhang, L.; Zhong, X.; Li, X.; Tian, Y.; Cheng, C.; Xu, B. Synergistic Effects of Multiple Functional Ionic Liquid-Treated PEDOT:PSS and Less-Ion-Defects S-Acetylthiocholine Chloride-Passivated Perovskite Surface Enabling Stable and Hysteresis-Free Inverted Perovskite Solar Cells with Conversion Efficiency Over 20%. *Nano Energy* **2019**, *63*, 19.103866.

(20) Geffroy, C.; Grana, E.; Bessho, T.; Almosni, S.; Tang, Z.; Sharma, A.; Kinoshita, T.; Awai, F.; Cloutet, E.; Toupance, T.; et al. p-Doping of a Hole Transport Material via a Poly(ionic

liquid) for over 20% Efficiency and Hysteresis-Free Perovskite Solar Cells. *ACS Appl. Ener. Mater.* **2020**, *3*, 1393-1401.

(21) Yin, X.; Song, Z.; Li, Z.; Tang, W. Toward Ideal Hole Transport Materials: A Review on Recent Progress in Dopant-Free Hole Transport Materials for Fabricating Efficient and Stable Perovskite Solar Cells. *Energy Environ. Sci.* **2020**, *13*, 4057-4086.

(22) Niu, T.; Chao, L.; Gao, W.; Ran, C.; Song, L.; Chen, Y.; Fu, L.; Huang, W. Ionic Liquids-Enabled Efficient and Stable Perovskite Photovoltaics: Progress and Challenges. *ACS Ener. Lett.* **2021**, 1453-1479.

(23) Hu, M.; Wu, X.; Tan, W. L.; Tan, B.; Scully, A. D.; Ding, L.; Zhou, C.; Xiong, Y.; Huang, F.; Simonov, A. N.; et al. Solvent Engineering of a Dopant-Free Spiro-OMeTAD Hole-Transport Layer for Centimeter-Scale Perovskite Solar Cells with High Efficiency and Thermal Stability. *ACS Appl. Mater. Interfaces* **2020**, *12*, 8260-8270.

(24) Zhang, Y.; Huang, B.; Hu, M.; Tan, B.; Huang, F.; Cheng, Y.-B.; Simonov, A. N.; Lu, J. Radical Doped Hole Transporting Material for High-Efficiency and Thermostable Perovskite Solar Cells. *J. Mater. Chem. A* **2022**, *10*, 10604-10613.

(25) Tan, S.; Huang, T.; Yavuz, I.; Wang, R.; Weber, M. H.; Zhao, Y.; Abdelsamie, M.; Liao, M. E.; Wang, H. C.; Huynh, K.; et al. Surface Reconstruction of Halide Perovskites During Post-treatment. *J. Am. Chem. Soc.* **2021**, *143*, 6781-6786.

(26) Akin, S.; Dong, B.; Pfeifer, L.; Liu, Y.; Graetzel, M.; Hagfeldt, A. Organic Ammonium Halide Modulators as Effective Strategy for Enhanced Perovskite Photovoltaic Performance. *Adv. Sci.* **2021**, *8*, 2004593.

(27) Alharbi, E. A.; Alyamani, A. Y.; Kubicki, D. J.; Uhl, A. R.; Walder, B. J.; Alanazi, A. Q.; Luo, J.; Burgos-Caminal, A.; Albadri, A.; Albrithen, H.; et al. Atomic-Level Passivation Mechanism of Ammonium Salts Enabling Highly Efficient Perovskite Solar Cells. *Nat. Commun.* **2019**, *10*, 3008.

(28) Cho, K. T.; Paek, S.; Grancini, G.; Roldán-Carmona, C.; Gao, P.; Lee, Y.; Nazeeruddin, M. K. Highly Efficient Perovskite Solar Cells with a Compositionally Engineered Perovskite/Hole Transporting Material Interface. *Energy Environ. Sci.* **2017**, *10*, 621-627.

(29) Jiang, Q.; Zhao, Y.; Zhang, X.; Yang, X.; Chen, Y.; Chu, Z.; Ye, Q.; Li, X.; Yin, Z.; You, J. Surface Passivation of Perovskite Film for Efficient Solar Cells. *Nat. Photonics* **2019**, *13*, 460-466.

(30) Kim, H.; Lee, S. U.; Lee, D. Y.; Paik, M. J.; Na, H.; Lee, J.; Seok, S. I. Optimal Interfacial Engineering with Different Length of Alkylammonium Halide for Efficient and Stable Perovskite Solar Cells. *Adv. Ener. Mater.* **2019**, *9*, 1902740.

(31) Kanda, H.; Shibayama, N.; Huckaba, A. J.; Lee, Y.; Paek, S.; Klipfel, N.; Roldán-Carmona, C.; Queloz, V. I. E.; Grancini, G.; Zhang, Y.; et al. Band-Bending Induced Passivation: High Performance and Stable Perovskite Solar Cells Using a Perhydropoly(silazane) Precursor. *Energy Environ. Sci.* **2020**, *13*, 1222-1230.

(32) Hu, S.; Pascual, J.; Liu, W.; Funasaki, T.; Truong, M. A.; Hira, S.; Hashimoto, R.; Morishita, T.; Nakano, K.; Tajima, K.; et al. A Universal Surface Treatment for p-i-n Perovskite Solar Cells. *ACS Appl. Mater. Interfaces* **2022**, *14*, 56290-56297.

(33) Scalon, L.; Szostak, R.; Araujo, F. L.; Adriani, K. F.; Silveira, J.; Oliveira, W. X. C.; Da Silva, J. L. F.; Oliveira, C. C.; Nogueira, A. F. Improving the Stability and Efficiency of Perovskite Solar Cells by a Bidentate Anilinium Salt. *JACS Au* **2022**, *2*, 1306-1312.

(34) Sidhik, S.; Wang, Y.; De Siena, M.; Asadpour, R.; Torma, A. J.; Terlier, T.; Ho, K.; Li, W.; Puthirath, A. B.; Shuai, X.; et al. Deterministic Fabrication of 3D/2D Perovskite Bilayer Stacks for Durable and Efficient Solar Cells. *Science* **2022**, *377*, 1425-1430.

(35) Tan, S.; Huang, T.; Yavuz, I.; Wang, R.; Yoon, T. W.; Xu, M.; Xing, Q.; Park, K.; Lee, D. K.; Chen, C. H.; et al. Stability-Limiting Heterointerfaces of Perovskite Photovoltaics. *Nature* **2022**, *605*, 268-273.

(36) Perini, C. A. R.; Rojas-Gatjens, E.; Ravello, M.; Castro-Mendez, A. F.; Hidalgo, J.; An, Y.; Kim, S.; Lai, B.; Li, R.; Silva-Acuna, C.; et al. Interface Reconstruction from Ruddlesden-Popper Structures Impacts Stability in Lead Halide Perovskite Solar Cells. *Adv. Mater.* **2022**, *34*, e2204726.

(37) Ma, C.; Kang, M. C.; Lee, S. H.; Zhang, Y.; Kang, D. H.; Yang, W.; Zhao, P.; Kim, S. W.; Kwon, S. J.; Yang, C. W.; et al. Facet-Dependent Passivation for Efficient Perovskite Solar Cells. *J. Am. Chem. Soc.* **2023**, *145*, 24349-24357.

(38) Nishimura, N.; Mathew, S.; Murakami, T. N. Suppressing Hydrogen Bonds and Controlling Surface Dipole: Effective Passivation for Hydrophobic Perovskite Photoabsorber Layers in Solar Cells. *New Journal of Chemistry* **2023**, *47*, 4197-4201.

(39) Suo, J.; Yang, B.; Mosconi, E.; Bogachuk, D.; Doherty, T. A. S.; Frohna, K.; Kubicki, D. J.; Fu, F.; Kim, Y.; Er-Raji, O.; et al. Multifunctional Sulfonium-Based Treatment for Perovskite Solar Cells with Less Than 1% Efficiency Loss Over 4,500-h Operational Stability Tests. *Nat. Energy* **2024**, *9*, 172-183.

(40) Noel, N. K.; Abate, A.; Stranks, S. D.; Parrott, E. S.; Burlakov, V. M.; Goriely, A.; Snaith, H. J. Enhanced Photoluminescence and Solar Cell Performance via Lewis Base Passivation of Organic-Inorganic Lead Halide Perovskites. *ACS Nano* **2014**, *8*, 9815-9821.

(41) Li, W.; Dong, H.; Wang, L.; Li, N.; Guo, X.; Li, J.; Qiu, Y. Montmorillonite as Bifunctional Buffer Layer Material for Hybrid Perovskite Solar Cells with Protection from Corrosion and Retarding Recombination. *J. Mater. Chem. A* **2014**, *2*, 13587-13592.

(42) Yue, Y.; Salim, N.; Wu, Y.; Yang, X.; Islam, A.; Chen, W.; Liu, J.; Bi, E.; Xie, F.; Cai, M.; et al. Enhanced Stability of Perovskite Solar Cells through Corrosion-Free Pyridine Derivatives in Hole-Transporting Materials. *Adv. Mater.* **2016**, *28*, 10738-10743.

(43) Habisreutinger, S. N.; Noel, N. K.; Snaith, H. J.; Nicholas, R. J. Investigating the Role of 4 ‐ Tert Butylpyridine in Perovskite Solar Cells. *Adv. Ener. Mater.* **2016**, *7*, 1601079.

(44) Tumen-Ulzii, G.; Auffray, M.; Matsushima, T.; Adachi, C. Unintentional Passivation of 4-Tertbutyl Pyridine for Improved Efficiency and Decreased Operational Stability of Perovskite Solar Cells. *Appl. Phys. Lett.* **2021**, *118*.

(45) Abate, A.; Leijtens, T.; Pathak, S.; Teuscher, J.; Avolio, R.; Errico, M. E.; Kirkpatrik, J.; Ball, J. M.; Docampo, P.; McPherson, I.; et al. Lithium Salts as "Redox Active" p-Type Dopants for Organic Semiconductors and Their Impact in Solid-State Dye-Sensitized Solar Cells. *Phys. Chem. Chem. Phys.* **2013**, *15*, 2572-2579.

(46) Pinkert, A.; Marsh, K. N.; Pang, S.; Staiger, M. P. Ionic Liquids and Their Interaction with Cellulose. *Chem. Rev.* **2009**, *109*, 6712-6728.

(47) Jeong, J.; Kim, M.; Seo, J.; Lu, H.; Ahlawat, P.; Mishra, A.; Yang, Y.; Hope, M. A.; Eickemeyer, F. T.; Kim, M.; et al. Pseudo-Halide Anion Engineering for Alpha-FAPbI(3) Perovskite Solar Cells. *Nature* **2021**, *592*, 381-385.